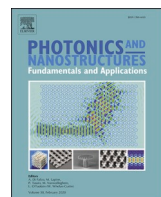




Contents lists available at ScienceDirect

# Photonics and Nanostructures - Fundamentals and Applications

journal homepage: [www.elsevier.com/locate/photonics](http://www.elsevier.com/locate/photonics)

## Editor's highlights

## Static and ultrafast optical response of two metal nanoparticles glued with a semiconductor quantum dot



Sabina Gurung <sup>a,b</sup>, Asha Singh <sup>a</sup>, Durga Prasad Khatua <sup>a,b</sup>, Himanshu Srivastava <sup>c</sup>, J. Jayabal <sup>a,b,\*</sup>

<sup>a</sup> Nano Science Laboratory, Materials Science Section, Raja Ramanna Centre for Advanced Technology, Indore 452013, India

<sup>b</sup> Homi Bhabha National Institute, Training School Complex, Anushakti Nagar, Mumbai 400094, India

<sup>c</sup> Lithography and Microscopy Laboratory, Synchrotrons Utilization Section, Raja Ramanna Centre for Advanced Technology, Indore 452013, India

## ARTICLE INFO

**Keywords:**

Localized surface plasmon resonance  
Hot-spot  
Dimer  
Hybrid nanostructures  
Gap plasmon  
Metal-semiconductor hybrids

## ABSTRACT

A hot-spot of high local field can be created between two closely placed metal nanoparticles and by irradiating them with an appropriate wavelength and polarization of incident light. The strength of the field at the gap between the particles is expected to get enhanced by several orders of magnitude higher than that of the applied field. Placing a semiconductor quantum dot or an analyte molecule at the hot-spot is an essential step towards harnessing the enhanced field for various applications. This article shows that it is possible to position a CdTe quantum dot (QD) between two larger silver nanospheres in a colloidal solution. The extinction spectra measured during growth suggests that the final hybrid nanostructure have two touching Ag nanoparticles (NPs) and a CdTe QD in between them close to the point of contact. Using ultrafast transient measurements, it has been shown that the presence of CdTe QD strongly influences the dynamics when the probe excites the gap plasmon. The method demonstrated here to place the semiconductor QD in between the two Ag NPs is an important step in the area of colloidal self-assembly and for the applications of hot-spot in plasmonic sensing, optoelectronics, energy-harvesting, nanolithography and optical nano-antennas.

## 1. Introduction

When excited at localized surface plasmon resonance (LSPR) the metal nanoparticle (NP) can significantly enhance the strength of electromagnetic field around them [1,2]. Such field enhancement can be as large as 20 times than that of the applied field [3]. This property of metal NP opened up its applications in plasmonic sensing, optoelectronics, energy harvesting, nanolithography, nano-antennas and imaging [4–12]. A second generation of local field enhancement is realized when two metal NPs are placed close to each other (dimer) with separation less than a few nanometers. Excitation of the dimer at a specific wavelength with polarization along the line joining the centers of the two particles can excite a plasmon mode known as “gap plasmon” [13,14]. When the gap plasmon is excited, the field in the gap between these two particles, known as the “hot-spot”, can get enhanced by a factor of five orders of magnitude than that of the applied [15–17]. Theoretical studies on the generation of such high field using two metal NPs of various size, shape, and orientation is being reported by various groups

[17,18]. In the past, bottom-up techniques such as chemical synthesis were used for the preparation of a large quantity of isolated metal NPs of different shapes with good size and crystal quality [19–21]. To generate hot-spot, these particles were simply aggregated in the colloid. Such random hot-spots in aggregates were also used for increasing the SERS signals from molecules [20]. Recently dimer shaped Ag NPs, which can show hot-spot, was prepared in colloidal form by controlled addition of linking polymer or salt to Ag nanosphere colloid. When mixed, the linker molecule acted as a glue to stick the two larger sized metal NPs. Because this glue is tiny, further attachment of metal NP to the same glue spot is prevented, creating the desired dimer structure [22,23]. There are other similar solution-based techniques to prepare dimers [24,25]. All these dimer preparation methods require a high level of control over the number of linking molecules versus the number of NPs to avoid large aggregates. Although such techniques allow the preparation of hot-spot, placing a semiconductor QD or an analyte molecule in that location is also important for harnessing the enhanced local field for applications. Once placed at the hot-spot, the material will experience a strong field

\* Corresponding author at: Nano Science Laboratory, Materials Science Section, Raja Ramanna Centre for Advanced Technology, Indore 452013, India.  
E-mail address: [jjaya@rrcat.gov.in](mailto:jjaya@rrcat.gov.in) (J. Jayabal).

leading to enhancement in its absorption, emission, and pronounced Fano-like effect, and so forth [26,27]. Yampolsky et al. could observe the motion of chemical bonds within a single molecule by placing it in between two gold NPs [28]. Placing a metal NP close to a highly reflecting substrate could also creates a similar situation as that of a dimer [29,30]. Studies on single molecule could also be carried out by placing it in between the metal NP and the surface [13,31].

In this article, we show that by mixing Ag NP colloid with TGA capped CdTe QDs in a particular mixing ratio, it is possible to prepare hybrid nanostructure with CdTe QD stuck in between the two Ag NPs. By comparing the measured extinction spectra during self-organized growth of the hybrid nanostructure with that of the calculated, we explain the process of hybrid formation. Ultrafast pump-probe measurements can provide quantitative information regarding complex processes that occurs between the metal and semiconductor nanocomposites. Using ultrafast transient transmission measurements, it has been shown that the carrier dynamics in the hybrid colloid is effected only when probed by a light that generates a high field in between Ag NPs. The method demonstrated here to place the semiconductor QD in between the two Ag NPs is an important step in the area of colloidal self-assembly and for application of gap plasmon in plasmonic sensing, optoelectronics, energy-harvesting, nanolithography and optical nanoantennas.

## 2. Experimental details

The individual constituents of the hybrid nanostructure, citrate capped silver NPs and TGA capped CdTe QDs dispersed in water, were prepared separately by wet-chemical methods [32–34]. The procedure followed for the preparation of this individual colloids has been reported earlier [35]. Ag-CdTe hybrid colloid, labeled H<sub>y</sub>, is prepared by mixing V<sub>p</sub>, volume of Ag NP colloid and V<sub>d</sub>, volume of CdTe QD colloid. Here the mixing ratio,  $\gamma$ , is defined as  $V_p/V_d$ . In the mixed solution, the Ag-CdTe hybrid nanostructures are expected to form because of self-organized growth [21,35–37]. A 1 kHz, 35 femtosecond oscillator-amplifier system (Coherent: Legend Elite HE +) was used for the transient transmission measurements in standard pump-probe geometry (Fig. 1). The pump beam (400 nm) for the experiment was obtained by generating the second-harmonic of part of the 800 nm beam from the laser system using a BBO crystal. The rest of the 800 nm beam was used for pumping an optical parametric amplifier (Coherent: TOPAS-800-fs). A fraction of the optical parametric amplifier output beam (408 nm or 550 nm) was used for probing the optical response of the sample. The polarization of the 408 nm and 550 nm beams was parallel and perpendicular to that of the pump beam, respectively. The pump fluence and the pulse width at the sample location is nearly  $2.1 \mu\text{J mm}^{-2}$  and 180 fs, respectively. The sample was circulated continuously in a 1 mm cell to avoid any thermal damage.

## 3. Results and discussion

Fig. 2 a shows the extinction spectrum of the individual Ag NP colloid and CdTe QD colloid. The extinction spectrum of the Ag NP colloid shows a single peak at 413 nm, which corresponds to the LSPR of small silver nanospheres dispersed in water [38,39]. The extinction spectrum of the CdTe QD colloid shows an exciton peak at 635 nm due to 1s(e)-1s(h) transition [40–42]. For structural characterization, few drops of these samples were dried on a mica substrate, and the topography of the surface was measured using an Atomic Force Microscope (AFM). Some representative AFM images of the individual colloids are shown in Fig. S1 of supporting information (SI). The AFM images that corresponds to individual Ag NP colloid and CdTe QD colloid show the presence of mostly well-separated particles. The average diameter of the Ag NPs and CdTe QDs measured using the height profile from these AFM images is 17 nm and 3.5 nm, respectively.

At the mixing ratio of  $\gamma = 50$ , there are about two Ag NPs for each CdTe QDs in the mixed colloid (see SI for details). The concentration of semiconductor QDs and metal NPs in the individual colloids can be estimated by using procedures reported by Yu et al. and Sriram et al. respectively [41,43]. The estimated number densities of CdTe QDs and Ag NPs in the corresponding individual colloids used in the preparation of hybrid are  $4.8 \times 10^{15} \text{ mL}^{-1}$  and  $1.2 \times 10^{14} \text{ mL}^{-1}$  respectively. These densities are also in agreement with the 2:1 number ratio of Ag NPs and CdTe QDs. Ag-CdTe hybrid sample, H<sub>50</sub>, was prepared by mixing CdTe QD colloid with Ag NP colloid at a mixing ratio of  $\gamma = 50$ . Immediately after the addition, the LSPR peak red-shifts slightly and at the same time the extinction peak height reduces to about 74% of that before addition (Fig. 2b). Although the red-shift is very small, repeated preparation shows that the red-shift does occur at about 1 min after mixing (Fig. S2). Over the period of the next few minutes, another peak appears on the red-side. For example, the spectrum of the sample taken after 2 min could be fit well with two Gaussian peaks (Fig. 3a). From 2 min to 10 min, the original LSPR peak blue-shifts and continues to reduce in strength. Whereas the longer wavelength peak red-shifts and grows (Fig. 2b). After about 10 min, the mixed colloid shows no further change in the spectrum. The final stable hybrid sample thus formed (H<sub>50</sub>) has peaks at 410 nm and 535 nm with strength 65% and 32% of that of bare Ag NP colloid, respectively. Note that the sample would be continuously evolving during the measurement of the spectra. Nevertheless, the measured spectra can be used for gaining insight into the hybrid formation process.

A self-organized growth of Ag-CdTe hybrid nanostructure is expected in the mixed sample because of the tendency of TGA to get attached to the surface of Ag NP [35,44,45]. As the TGA is already attached to the CdTe QD, these QDs are also brought in close proximity to the Ag NPs [35,44,45]. The final structure of the hybrid formed by the self-organized growth process depends on the ratio between the number of Ag NPs and CdTe QDs in the mixture, properties of the capping agents, size, and shape of the individual particles. When Ag NP and CdTe QD colloids are mixed in a ratio of  $\gamma = 0.56$ , hybrid nanostructures of Ag NP

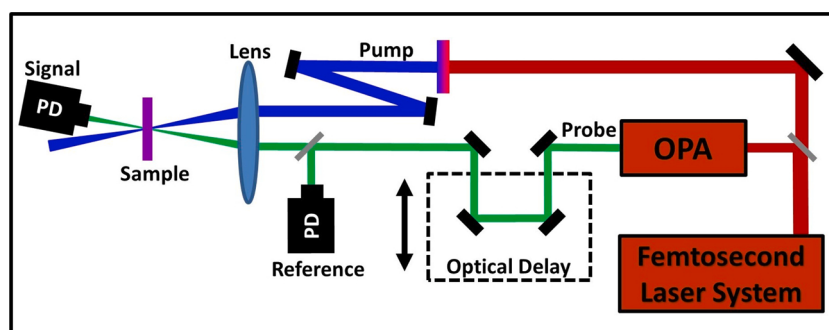
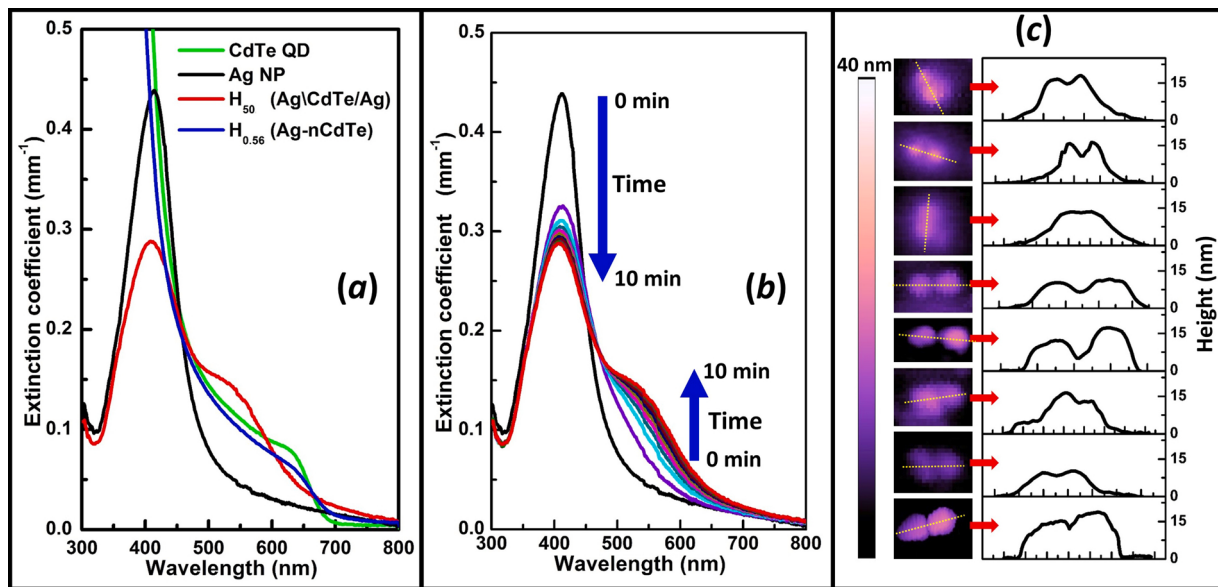
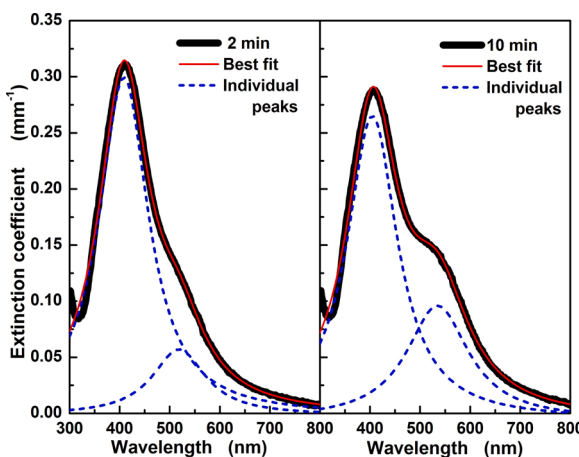


Fig. 1. Schematic of the pump-probe setup used for the measurement of transient transmission in the samples.



**Fig. 2.** Static optical and structural characterization of individual, mixed and hybrid colloids: (a) Extinction coefficient of CdTe QD, Ag NP, H<sub>50</sub> hybrid and H<sub>0.56</sub> hybrid colloids. (b) The time evolution of extinction spectrum of the mixed colloid from just after mixing to about 10 min. (c) Representative AFM images of hybrid nanostructures present in the H<sub>50</sub> hybrid colloid. x is the distance along the substrate surface.



**Fig. 3.** Extinction spectrum of the mixed sample (black lines) after (a) 2 min and (b) 10 min. Best fit to these experimental spectra using two Gaussian peaks (red lines). The contribution from individual peaks are also shown (blue lines).

surrounded by nearly 45 CdTe QDs (H<sub>0.56</sub> or Ag-nCdTe) are formed [35]. Once the CdTe QDs surround the Ag NP completely, it prevents further attachment of CdTe QD to the Ag NP, thus making the final hybrid structure stable. The extinction spectrum of the H<sub>0.56</sub> sample thus formed is also shown in Fig. 2a for comparison. Clearly the extinction spectrum of this H<sub>0.56</sub> sample is very different from that of the H<sub>50</sub> sample. The H<sub>0.56</sub> has an increasing absorption strength towards UV similar to that of bare CdTe QD colloid. On the other hand the H<sub>50</sub> sample shows a dip in absorption around 320 nm, which resembles more of an Ag NP colloid. The AFM images of the H<sub>50</sub> sample dried on mica-substrate shows several twin particles of each having nearly 17 nm height (Fig. 2c). Based on the height, each of these particles should be the Ag NPs present in the mixed colloid. Further, based on the number density ratio and the tendency of TGA to get attached to the Ag surface [44,45], we propose that in the final hybrid colloid, there are nanostructures with two Ag NPs attached to a single CdTe QD.

If a mixed hybrid sample was prepared with a mixing ratio  $\gamma$  higher than 50, stable colloids do get formed. The final extinction spectrum of

these hybrid colloids ( $\gamma > 50$ ) has an extinction spectrum that looks similar to that observed in the intermediate stages (Fig. 2b). For these  $\gamma$  values, there will not be enough CdTe QDs to join all the Ag NPs leaving several unattached Ag NPs along with few H<sub>50</sub> hybrids [35]. On the other hand, if the mixing ratio is lower than 50, aggregated nanostructures were found to settle down at the bottom of the sample. This can be explained by the presence of excess CdTe QDs, which can link several H<sub>50</sub> forming large chain-like structures that eventually become heavy enough to settle down [46,47].

To understand the time evolution of the measured extinction spectra after mixing and to further understand the structure of the final hybrid formed, optical response of various Ag-CdTe hybrid nanostructures were numerically calculated using T-matrix technique (Fig. 4). T-matrix is a numerical method for computing the optical response of a collection of spherical particles [48,49]. For Ag NPs of the size of the order of 17 nm, quantum confinement effects can be neglected, and hence experimental bulk dielectric constants were used for the optical response calculations [50]. On the other hand, the dielectric constant of a CdTe QD of size 3.5 nm will be substantially different from that of its bulk because of the

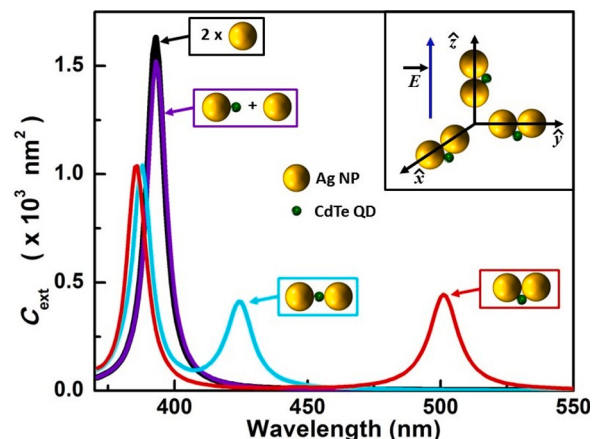


**Fig. 4.** Calculated extinction cross-section of two non-interacting Ag NPs, attached Ag-CdTe particles, chain of Ag-CdTe-Ag particles and touching Ag-Ag particles with CdTe QD on one side.

quantum confinement effect [51]. The dielectric constant of CdTe QD was estimated using the method reported by Marcelo Alves-Santos et al., which uses the measured extinction spectrum and a trial and error procedure [51]. In the colloidal solution, it is expected that particles will be oriented in all possible directions. To mimic that situation with minimal computational cost, the extinction spectrum is estimated by averaging the responses calculated for a given field direction and particles aligned along the three Cartesian directions (see inset of Fig. 4) [49,52].

The calculated extinction cross-section of the Ag NP shows a single peak at 393 nm (Fig. 4). To compare with the other structures, where there are two Ag NPs involved,  $C_{ext}$  of the two isolated Ag NPs (same as the cross-section of single Ag NP multiplied by two) is plotted in Fig. 4. Once the Ag NP and the CdTe QD colloids were mixed, the most possible situation would be that a single CdTe QD will get attached to a single Ag NP. The second Ag NP would not have joined yet. To mimic such a situation, we have calculated  $C_{ext}$  of a single CdTe QD attached with an Ag NP and another Ag NP placed sufficiently away from it. The  $C_{ext}$  thus obtained shows a red-shift of about 1 nm when compared to that of isolated Ag NP. Further, the peak height also reduces to about 90% of that of two isolated Ag NPs. Attaching a higher refractive index material to a metal NP is known to red-shift its LSPR peak [53,54]. The changes in  $C_{ext}$ , the red-shift and the reduction in peak strength, when CdTe is attached to one of the Ag NP matches well with the observed change in the extinction spectrum measured at nearly a minute after mixing Ag NP and CdTe QD colloids (Fig. 2(b)). When another Ag NP is attached to the other end of CdTe QD which is already attached to an Ag NP, it will result in the formation of a linear Ag-CdTe-Ag structure. The  $C_{ext}$  of this structure shows a new peak at 424 nm and the original LSPR peak, which was at 393 nm blue-shifts by 5 nm to 388 nm. These LSPR peaks, 424 nm and 388 nm, appear when the field is aligned along the line joining the centers of the two Ag spheres (longitudinal axis) and perpendicular to it (transverse axis) respectively (Fig. 4). Fitting the measured extinction spectrum at 2 min after mixing shows a double peak structure, which matches well with that of  $C_{ext}$  of Ag-CdTe-Ag (Fig. 3). The final spectrum ( $>10$  min) of the hybrid has a second peak at 535 nm which is much more red-shifted than that calculated for the Ag-CdTe-Ag structure. Although capping prevents Ag NPs to join together, once brought in close proximity to each other, the metal NP do tend to join and restructure themselves [55–57]. Thus, once joined by the CdTe QD it is possible that over time the linear Ag-CdTe-Ag hybrid changes its structure to that with two Ag NPs touching each other with CdTe QD pushed to one side (Ag\CdTe/Ag) as shown in Fig. 4. The calculated  $C_{ext}$  of Ag\CdTe/Ag hybrid match closer to the experimentally observed final extinction spectrum which has peaks at 408 nm and 535 nm (Fig. 2a). Thus the peak at 408 nm corresponds to the LSPR originating when the field is aligned along the transverse axis (T-LSPR). Similarly the 535 nm peak corresponds to the LSPR when field is aligned along the longitudinal axis (L-LSPR).

Another effective tool to understand the origin of various plasmon peaks arising in a collection of interacting small metal NPs like dimer, trimer, etc., is plasmon hybridization model [58]. However, this model cannot in general be used for estimating the optical response of metal NPs in presence of CdTe QDs [59]. The result of T-Matrix calculations (which is applicable for a collection of spheres of any materials [49]), shows that the extinction spectrum of Ag-CdTe-Ag and Ag\CdTe/Ag is slightly different from that of the corresponding structures without CdTe QD (Fig. S7). Although plasmon hybridization model could be used to understand the final response of interaction between metal NPs, more realistic modes and resonance of the dimer like structures in the presence of CdTe QDs requires calculation like T-matrix or finite-difference time-domain.

Comparing the measured temporal evolution of the extinction spectra (Fig. 2b) and the calculated optical responses of the Ag NP and hybrid nanostructures (Fig. 4), the growth of the final hybrid nanostructure can now be explained. Just after mixing, CdTe QD gets

attached to Ag NP forming a large number of hybrid nanostructures each with one Ag NP and one CdTe QD. Such an Ag-CdTe hybrid structure coexists in the colloidal solution along with an almost equal number of unattached Ag NPs. This is indicated by the observed small red-shift and reduction in strength of the LSPR peak when measured 1 min after mixing (Fig. S2). As time progresses, another Ag NP also gets attached to the Ag-CdTe nanostructure to form an Ag-CdTe-Ag linear hybrid nanostructure. The observed second peak on the red-side of the extinction spectra measured in the first few minutes indicates the formation of such structures. Followed by this, the linear Ag-CdTe-Ag structure realign themselves to form a Ag\CdTe/Ag structure. This explains the observed red-shifting of the long-wavelength peak, which finally settles down at 535 nm. To further confirm these observations, we have also prepared Ag\CdTe/Ag hybrids with larger Ag NPs with a diameter of nearly 50 nm (Fig. S4). Once again, the experimental results match well with that of the calculated spectra using T-matrix. Thus the final stable colloid, H<sub>50</sub> should have hybrid NPs of Ag\CdTe/Ag structure. The size of the CdTe QD is much smaller and is now in between two large Ag NPs, thus further attachment of Ag NP to the same CdTe QD is prevented. Because of the limitation in resolution, the AFM image could not resolve the presence of small CdTe QD sitting between the larger Ag NPs. Hence the AFM images of the Ag\CdTe/Ag hybrid could only show a Ag NP dimer-like structure (Fig. 2c). In some of the AFM images of H<sub>50</sub>, we also find few hybrid structures with Ag NPs attached to each other in a triangular formation and few Ag NPs in chain-like structure (inset of Fig. S3). The T-matrix calculation shows that these triangular and chain-like structures have a very different extinction spectra than those observed in the experiment (Fig. S3).

The efficiency of Ag\CdTe/Ag nanostructure formation in this synthesis process could be obtained by the number density of nanostructures observed in AFM images as well as by comparing the calculated extinction spectra of the individual nanostructures with that of experimentally measured hybrid colloid. Note that the AFM measurements were performed on a mica substrate over which few drops of the hybrid colloid is dried. The structure of the nanoaggregates found on the mica substrate could depend on the number density of particles in colloid, the properties of the colloid and substrate and also on the drying process itself. Thus, AFM image only gives a representation of the nanostructures floating in the colloidal solution. On the AFM images, we find that the ratios of monomers:dimers:trimers:chain to be 4:16:2:1. The T-Matrix calculation shows that in case of dimers, the ratio between the peak strengths of the two LSPR peaks is 0.43. For trimer and chain of particles, the ratio between the two strongest peaks (which are also close to the LSPR peaks of dimer) is 0.6 and 1 respectively. While for the monomer there should not be any longer wavelength peak. The ratio between the two peaks in the experimental extinction spectrum of Ag\CdTe/Ag hybrid is 0.49, which is close to that of dimer. Meanwhile, an estimated spectrum of mixed colloid containing monomers, dimers, etc. in the number ratios measured by AFM image is completely dominated by that of dimers (Fig. S6). Transmission electron microscope (TEM) could also be used for studying the structure of final self-aggregated Ag\Cdte/Ag nanostructures. Fig. 5 shows some of the TEM images of the colloid containing Ag\Cdte/Ag hybrid nanostructures. The presence of the capping agents (polymers) in a hybrid sample makes the process of capturing TEM images very difficult. Removal of these polymers by centrifuging would destroy the hybrid nanostructure present in the colloidal solution. Further, during TEM studies, the measurement had to be performed at very low irradiation, and the images had to be accrued quickly. Even then sometimes during the measurement, we still find that the particle disappear during image acquisition. The TEM images of Ag\Cdte/Ag hybrid nanostructures clearly shows the presence of a smaller particle (size in the range of CdTe QDs) in between two larger-sized particles (size of the order of Ag NPs) which matches well with that of expected from optical characterization (Fig. 5).

It is interesting to note that the observed strengths of the LSPR peaks in the case of Ag\CdTe/Ag hybrid colloid can be explained by a simple

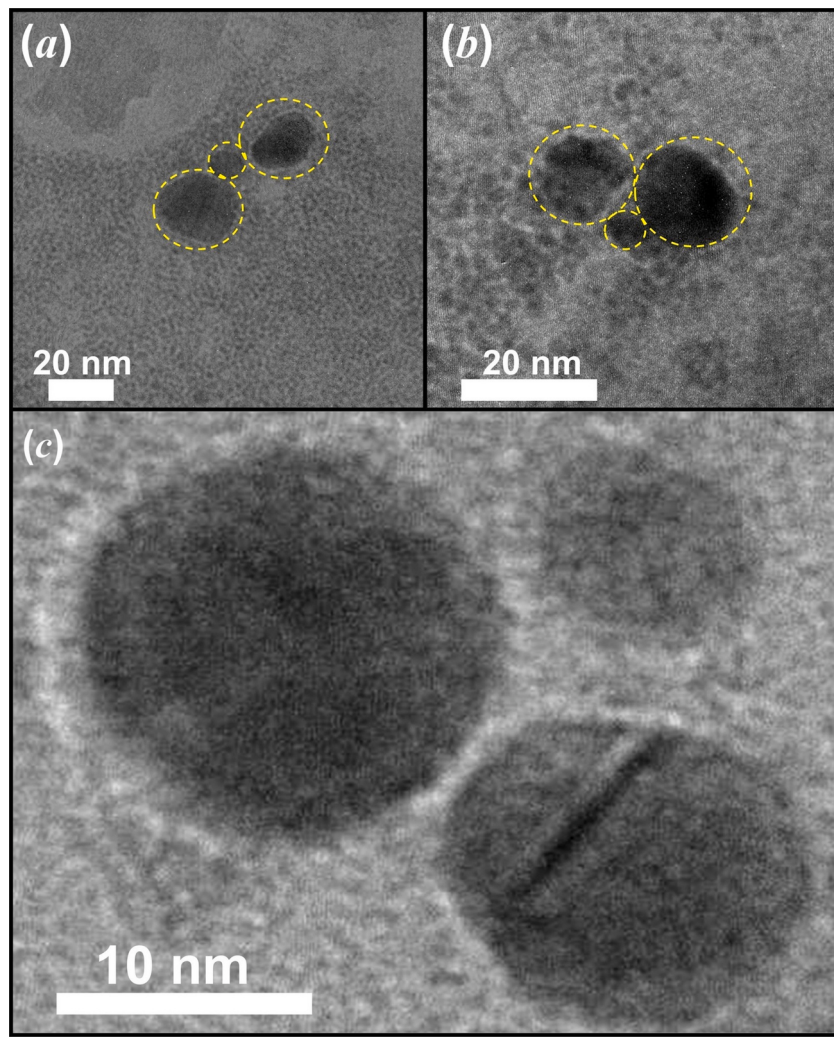


**Fig. 5.** TEM images of Ag\CdTe/Ag hybrid nanostructures.

model based on the orientation of the particles. Because of spherical symmetry, all the Ag NPs in the colloid absorbs the incident light irrespective of its polarization. Although in a colloidal sample all orientations of Ag\CdTe/Ag NP is possible, consider a more straightforward picture where all the particles are randomly aligned parallel to one of the three Cartesian directions with equal probability (inset of Fig. 4). Such an assumption in the distribution of particles has been shown to match well with that of the measured optical response of colloid containing randomly oriented ellipsoids and nanoprisms [46,52]. Let the electric field be aligned to one of the Cartesian directions such that about 66.7% ( $\frac{2}{3}$ ) of the particles will contribute to the T-LSPR peak (at 410 nm) because for these particles the polarization of light is oriented along the transverse axis. Whereas the rest 33.3% ( $\frac{1}{3}$ ) of the particles have their longitudinal axis aligned along the polarization and will show resonance at L-LSPR (535 nm) i.e. along the gap plasmon. The measured LSPR peak heights for Ag\CdTe/Ag hybrid colloid at 410 nm and 535 nm are 65% and 32% of that of Ag NP colloid at its LSPR peak which are very close to that predicted by the model. This also implies that the  $C_{ext}$  of an Ag\CdTe/Ag particle is exactly the same as that of two isolated Ag NPs if polarization is appropriately aligned. The random orientations of the particles mainly cause the reduction in  $C_{ext}$  of the Ag\CdTe/Ag hybrid colloid.

Figs. 6 and 7 shows the transient transmission signal ( $\Delta T/T$ ) measured for the bare Ag NP and Ag\CdTe/Ag hybrid when probed at 408 nm and 550 nm, respectively. In all these measurements, the pump

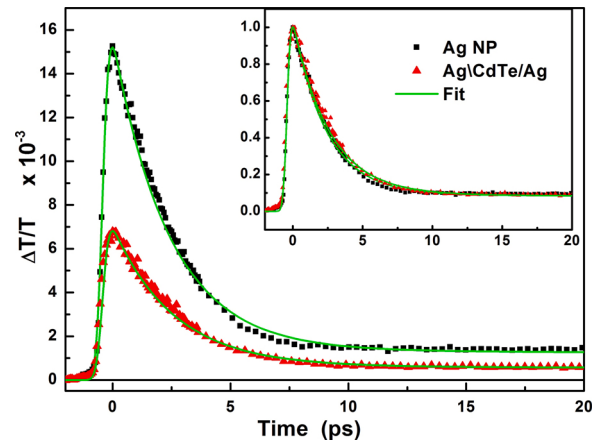


**Fig. 6.** Transient curve of Ag NPs and Ag\CdTe/Ag hybrid colloidal samples excited at 400 nm and probed at 408 nm. Inset shows the normalized transient curve of these samples.

wavelength (400 nm) and pump fluence ( $2.1 \mu\text{Jmm}^{-2}$ ) at the sample place were kept the same. For both the samples and at both probe wavelengths, the magnitude of  $\Delta T/T$  ( $|\Delta T/T|$ ) increases, reaching a maximum by about 400 fs. With further increase in the pump-probe delay,  $|\Delta T/T|$  starts recovering, reaching a very low value by about

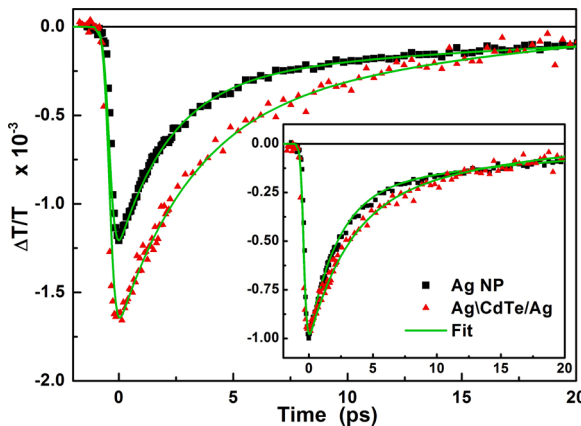


**Fig. 7.** Transient transmission curve of Ag NPs and Ag\CdTe/Ag hybrid colloidal samples excited at 400 nm and probed at 550 nm. Inset shows the normalized transient curve of these samples.

20 ps. Further, we find that sample containing bare CdTe QD colloid of concentration similar to that used in the preparation of the Ag\CdTe/Ag hybrid colloid did not show any measurable  $\Delta T/T$  signal.

The origin of the ultrafast optical response of the bare metal NP colloid has been reported by several groups [60–64]. When an ultrashort pulse excites a metal NP at its LSPR, the free-electrons in the particles are set to oscillate in phase with the applied field. Within the next few femtoseconds, these electrons decay to single-particle states through Landau-damping [60]. The energy distribution among electrons at this stage will be non-thermal. These electrons relax to a thermalized high-temperature state mainly through electron-electron scattering by about a few hundreds of femtoseconds [62]. With the increase in temperature of free-electrons, the real part of the dielectric constant of Ag also increases which red-shifts the LSPR peaks [62–64]. This shift causes a change in the transmission of a metal NP colloid. The peak change in the transient transmission occurs at the time when there is a maximum change in temperature of the free-electrons. In the present case of bare Ag NP colloid, when excited at 400 nm, the peak in  $|\Delta T/T|$  occurs nearly after 400 fs irrespective of probe wavelength. Further, the red-shift of LSPR will cause an increase in transmission, when probed at 408 nm (blue-side of LSPR), and reduction in transmission when probed at 550 nm. Thus, the difference in probing wavelength with respect to LSPR causes the change in the sign of the measured  $\Delta T/T$  in the case of Ag NP colloid (Figs. 6 and 7).

At the end of thermalization, the temperature of free-electrons is much higher, whereas the lattice still remains almost at room temperature. Over a time of next few picoseconds, electron-phonon interaction leads to the thermalization of electrons and lattice to a much lower temperature. This is because the specific heat capacity of the lattice is much higher than that of electrons. The thermalization process of electrons and lattice can be quantitatively understood using two-temperature model [62–64]. However, the two-temperature model would not be, in principle, directly applicable for hybrid nanostructures. In the present case, because hybrid nanostructures are also under study, the complete temporal evolution of  $\Delta T/T$  was fitted to,

$$F(t) = \frac{1}{2} [\mathcal{E}(t/t_r) + 1] \left[ \sum_k A_k e^{-t/t_k} \right] \quad (1)$$

where  $\mathcal{E}(x)$  is the Gauss error function of  $x$ ,  $A_k$  and  $t_k$  are the amplitude and decay time, respectively. The best fit to the experimental data using Eq. (1) is also shown in Figs. 6 and 7. In the case of the bare Ag NP colloid, the best fit value of electron-phonon thermalization time ( $\tau_{ep}$ ) probed at 408 nm and 550 nm are  $2.3 \text{ ps} \pm 0.1 \text{ ps}$  and  $2.4 \text{ ps} \pm 0.1 \text{ ps}$ , respectively.

Similar to the bare Ag NP colloid, the sign of  $\Delta T/T$  of Ag\CdTe/Ag

hybrid colloid also changes from positive to negative when probe wavelength is changed from 408 nm to 550 nm. This shows that the transient response of Ag\CdTe/Ag is strongly similar to that of pure Ag NP colloid. To compare the temporal response,  $\Delta T/T$  normalized to the peak change in  $|\Delta T/T|$  ( $|\Delta T/T|_{pk}$ ) are also shown in the inset of Figs. 6 and 7. The best fit to the decay times of  $\Delta T/T$  for Ag\CdTe/Ag hybrid colloid when probed at 408 nm and 550 nm are  $2.6 \text{ ps} \pm 0.1 \text{ ps}$  and  $3.2 \text{ ps} \pm 0.1 \text{ ps}$ , respectively. Clearly, when probed at 408 nm, the recovery of change in transmission of the Ag\CdTe/Ag hybrid colloid is slightly slower than Ag NP colloid, whereas, at 550 nm, it takes much longer to recover.

Electron-phonon relaxation takes a longer time in a single crystal Ag NP compared to that of a crystal having twin defects because of the additional scattering of electrons at the lattice defects [19]. In the present case, the lattice quality of the bare Ag NPs and Ag\CdTe/Ag hybrid colloids should be the same because the latter is derived from the former. Further, the simple linking of Ag NPs by the CdTe QD should not change its crystal quality. Thus the increase in the relaxation time of the Ag\CdTe/Ag hybrid colloid cannot be explained by assuming a modification in Ag crystal quality. At low temperatures, the electron-phonon relaxation time also depends on its temperature itself, increasing linearly with it [61]. Thus if the increase in the temperature of Ag in the Ag\CdTe/Ag hybrid nanostructure is more, then it can also show an increased electron-phonon relaxation time. The comparison between the measured  $|\Delta T/T|_{pk}$  for different samples will be able to give some information about the maximum temperature reached by the free-electrons in the Ag NPs. If  $\Delta\epsilon'_m$  is the small change in real part of dielectric constant due to the change in electron temperature, then the change in transmission at the probe wavelength ( $\Delta T/T$ ) of a colloid having randomly oriented ellipsoidal particle can be written as [64,61],

$$\frac{\Delta T}{T} = \frac{2\pi p}{3\lambda_{pr}\sqrt{\epsilon_s}} \sum_{j=x,y,z} \text{Im} \left[ f_j^2(\lambda_{pr}) \right] \Delta\epsilon'_m(\lambda_{pp}, \lambda_{pr}). \quad (2)$$

where  $p$  is the volume fraction,  $\epsilon_s$  is the dielectric constant of the surrounding medium,  $f_j$  is the local field factor for  $j^{th}$  principle axis [1]. Because the change in dielectric constant is induced by the pump pulse and is sensed at probe wavelength,  $\Delta\epsilon'_m$  should depend on both the pump and probe wavelengths and their polarizations with respect to the orientation of the particle. For sufficiently small absorbed pump energies,  $\Delta\epsilon'_m$  depends linearly on absorbed power per unit volume of the particle [64]. For small particles, the contribution to the extinction cross-section is mainly dominated by absorption. Thus,  $\Delta\epsilon'_m$  is expected to be directly proportional to the extinction cross-section of the particle.

The  $|\Delta T/T|_{pk}$  of Ag NP colloid when probed at 550 nm is much lower (only 9%) than that when probed at 408 nm. When pumped at 400 nm, irrespective of the polarization, all the Ag NPs absorbs the light. The change in the temperature of free-electrons will be proportional to the  $C_{ext}$  of a single Ag NP. When probed at 408 nm, all the Ag NPs will contributes to the  $|\Delta T/T|_{pk}$  and the contribution from  $\text{Im}[f_j^2]$  is also strong near to the LSPR (Fig. 8a). However, when probed at 550 nm which is far separated from LSPR, the contribution to  $|\Delta T/T|_{pk}$  from  $\text{Im}[f_j^2]$  reduces considerably [64–66], reducing the measured  $|\Delta T/T|_{pk}$ . Because the pump fluence is the same in both of these cases, the decay time will also remain the same irrespective of the probe wavelength.

Consider the simple model of Ag\CdTe/Ag particles oriented along the three Cartesian directions. In Fig. 8, schematic of particles oriented in three different directions along with the polarization of the pump and probe beams used in the experiments are shown. As discussed in the case of static optical response, when the particle is aligned along the transverse axis, its  $C_{ext}$  will remain nearly the same as that of two isolated Ag NPs. Thus when excited at 400 nm, close to T-LSPR, nearly  $\frac{2}{3}$  of the Ag\CdTe/Ag hybrid particles will absorb the light, and the increase in

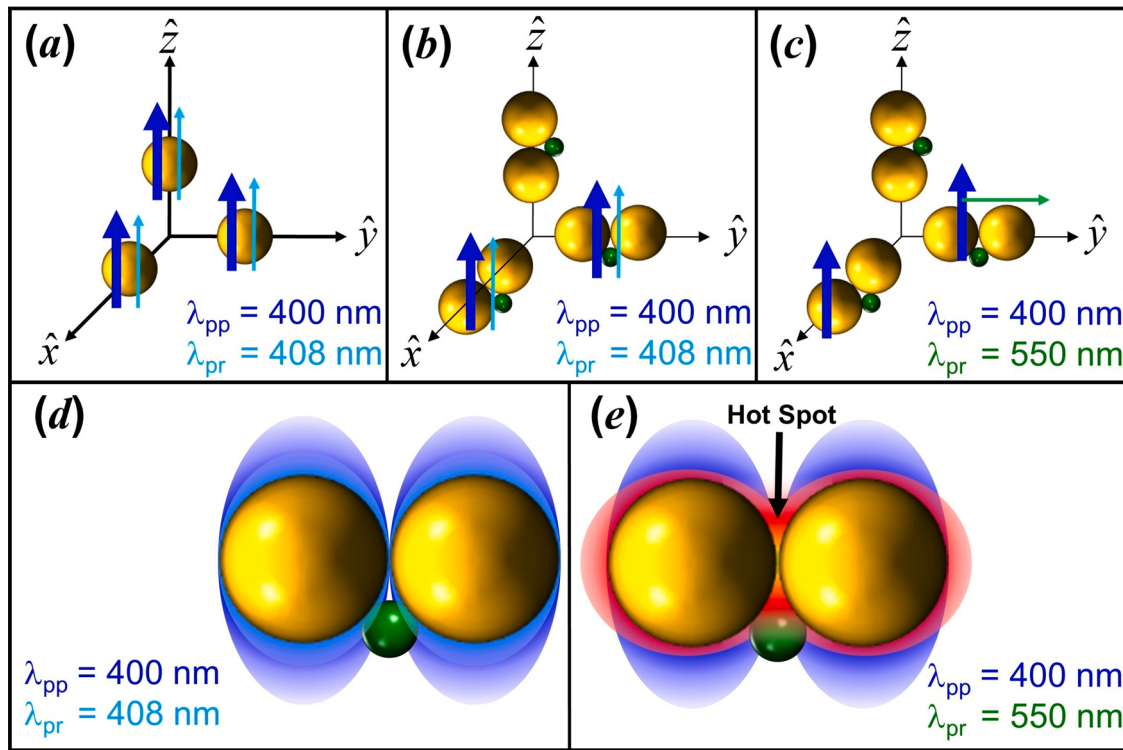


**Fig. 8.** Schematic of particles oriented in three different directions along with polarization of pump and probe pulse. Blue thick line indicates polarization of pump pulse (400 nm) and thin line, blue (408 nm) and green (550 nm), indicates polarization of probe pulse.

temperature of free-electrons will also be nearly same as that of the isolated Ag NP for the same pump fluence. When probed at 408 nm, the factor  $\text{Im}[f_j^2]$  will also be finite and all the excited Ag/CdTe/Ag particles (which is only  $\frac{2}{3}$  of the total) will contribute to  $|\Delta T/T|_{\text{pk}}$ . Thus the  $|\Delta T/T|_{\text{pk}}$  measured for Ag/CdTe/Ag hybrid colloid should be lesser by at least a factor of  $\frac{2}{3}$  compared to that of Ag NP colloid when probed at 408 nm. With a similar argument it can be shown that the  $|\Delta T/T|_{\text{pk}}$  of Ag/CdTe/Ag hybrid colloid probed at 550 nm, close to L-LSPR, should be lesser by at least a factor of  $\frac{1}{3}$  compared to that of Ag NP colloid probed at 408 nm (Fig. 8c). The  $|\Delta T/T|_{\text{pk}}$  measured for the Ag/CdTe/Ag hybrid colloid is about  $\sim 44\%$  and  $11\%$  when probed at 408 nm and 550 nm, respectively, compared to that of Ag NP colloid at 408 nm. Thus, the measured  $|\Delta T/T|_{\text{pk}}$  of Ag/CdTe/Ag hybrid colloid at these wavelengths was even lower than that estimated. Based on this observation, the increase in temperature of free-electrons in the Ag NPs of Ag/CdTe/Ag hybrids should be same or lower than that of the particles in bare Ag NP colloid. Thus the electron-phonon relaxation time measured for Ag/CdTe/Ag hybrid colloid should have remained the same or reduced than that of Ag NP colloid, which is opposite to that of observed in the experiment. Hence, change in the absorbed power cannot explain the increase in the relaxation time measured for Ag/CdTe/Ag hybrid colloid.

Prashant K. Jain et al. studied the transient change in the optical response of aggregated gold NPs when excited at 400 nm [67]. Their result shows that the electron-phonon relaxation time is shorter when probed at the longer-wavelength LSPR peak compared to that measured at the shorter wavelength. They attributed this reduction to the increased overlap of the longer wavelength LSPR with the phonon spectrum and the enhanced interfacial electron scattering [67]. A similar reduction in electron-phonon relaxation time has also been reported for other Au and Ag NP aggregates [68,69]. This implies that the interaction between two metal NPs should lead to a reduction in the relaxation time of the  $\Delta T/T$ , which is again the opposite of what is

observed in the present case. Thus, the presence of CdTe QD in between the Ag NPs is indeed playing a role in the dynamics observed in Ag/CdTe/Ag colloid.

When a metal NP is attached to a semiconductor, three processes start modifying the response of the combined superstructure. A direct metal-to-semiconductor interfacial charge transfer, which occurs through direct excitation of electron from metal NPs to empty states in semiconductor [70–72]. Such transfer is possible in hybrid systems where the semiconductor is in direct contact with the surface of the metal. In some hybrid cases, the metal NP absorbs the light creating hot-electrons, which then gets transferred to the empty levels in semiconductor. Signature of such hot-electron transfer from metal NP to semiconductor QD has been observed in several hybrid nanostructures [70,71,73]. Even if there is no direct contact between the metal and semiconductor, hot-carrier transport still occurs via the linking polymer/molecule [38,61]. In addition to the processes mentioned above, a direct energy transfer between metal and semiconductor is also possible, if the LSPR of metal NP overlaps with the absorption spectrum of semiconductor QD [74,75].

Charge or energy transfer between the constituents of a hybrid strongly depends on the final superstructure formed by the metal-semiconductor nanostructures [38,61,76]. When the Ag/CdTe/Ag hybrid colloid is pumped at 400 nm, T-LSPR is excited in the Ag NPs, and at the same time, it can also excite carriers in CdTe QD from valance band to conduction band. A comparison of temporal response of  $\Delta T/T$  of Ag NP colloid and Ag/CdTe/Ag colloid when probed at 408 nm shows that the dynamics in this system is dominated by the plasmonic response of Ag NP. Even if carriers are excited in CdTe QDs, when probed well above the band edge, CdTe QDs do not show a significant change in its transient response [38]. Further, exciting at 400 nm, resonant with T-LSPR, does not create hot-spot between the Ag NPs where CdTe QD is located since it does not excite gap plasmon (Fig. 8d). Thus probing the Ag/CdTe/Ag colloid at 408 nm strongly resembles the dynamics of Ag NP colloid (Fig. 6). On the other hand, when probed at 550 nm, the probe pulse can sense the presence of CdTe QD because the probe field

gets enhanced at the location of CdTe QD. Further, CdTe QD can also show a strong transient change in transmission when probed at 550 nm. Thus, although a significant contribution of metallic response is expected near to the gap plasmon, the Ag\CdTe/Ag hybrid colloid, when probed at 550 nm, shows a longer response time than that of bare Ag NP colloid.

#### 4. Conclusion

When Ag NP colloid is mixed with TGA capped CdTe QD colloid such that in the mixed colloid the number ratio between the Ag NPs and CdTe QDs is 2:1, stable hybrid nanostructure with two Ag NPs and a CdTe could be formed. Optical spectra during growth and transient optical response suggests that the final structure has two touching Ag NPs with CdTe QD stuck in between them. The static optical response of the final hybrid colloid could be explained well by the electromagnetic interaction between these particles present in the structure. Assuming that the extinction cross-section of each Ag NP in the Ag\CdTe/Ag hybrid structure to be the same as that of an isolated Ag NP, the optical response of Ag\CdTe/Ag colloid could be explained by their random orientations in the host. When excited and probed near the T-LSPR, the ultrafast optical response of Ag\CdTe/Ag hybrid nanostructure resembles that of a bare Ag NP. On the other hand, when probing at the gap plasmon, a delayed recovery of transient transmission was observed. This is attributed to sensing the presence of CdTe QD in the hot-spot regime by the probe field tuned to the gap plasmon. Placing a semiconductor QD at or close to the hot-spot is a significant step towards using the enhanced local field in various applications such as plasmonic sensing, optoelectronics, energy harvesting, nanolithography and optical nano-antennas. A similar hybrid formation technique can be extended to other noble metals and II-VI semiconductor quantum dots capped with thiols. Therefore these studies are also crucial for the advancement in the area of colloidal self-assembly, with impacts on the dynamic properties of gap plasmon for specific needs [77,78].

#### Declaration of interests

None.

#### Declaration of Competing Interest

The authors report no declarations of interest.

#### Acknowledgments

The authors are thankful to Tarun Kumar Sharma, Rama Chari and Salahuddin Khan for fruitful discussions and suggestions. The authors are also thankful to Arvind Kumar Srivastava for the support in obtaining the TEM images. The authors, Sabina Gurung and Durga Prasad Khatua are thankful to RRCAT, Indore, under HBNI programme, Mumbai, for the financial support.

#### Appendix A. Supplementary data

Supplementary data associated with this article can be found, in the online version, at <https://doi.org/10.1016/j.photonics.2020.100869>.

#### References

- [1] C.F. Bohren, D.R. Huffman, *Absorption and Scattering of Light by Small Particles*, John Wiley & Sons, 2008.
- [2] P. Bharadwaj, P. Anger, L. Novotny, Nanoplasmonic enhancement of single-molecule fluorescence, *Nanotechnology* 18 (4) (2006) 044017.
- [3] M. Futamata, Y. Maruyama, M. Ishikawa, Local electric field and scattering cross section of Ag nanoparticles under surface plasmon resonance by finite difference time domain method, *J. Phys. Chem. B* 107 (31) (2003) 7607–7617.
- [4] K. Catchpole, A. Polman, Plasmonic solar cells, *Opt. Express* 16 (26) (2008) 21793–21800.
- [5] J.A. Ruemmele, W.P. Hall, L.K. Ruvuna, R.P. Van Duyne, A localized surface plasmon resonance imaging instrument for multiplexed biosensing, *Anal. Chem.* 85 (9) (2013) 4560–4566.
- [6] H.A. Atwater, A. Polman, *Plasmonics for improved photovoltaic devices*, *Materials For Sustainable Energy: A Collection of Peer-Reviewed Research and Review Articles from Nature Publishing Group* (2011) 1–11.
- [7] S.K. Cushing, N. Wu, Plasmon-enhanced solar energy harvesting, *Electrochim. Soc. Interface* 22 (2) (2013) 63–67.
- [8] R. Jiang, B. Li, C. Fang, J. Wang, Metal/semiconductor hybrid nanostructures for plasmon-enhanced applications, *Adv. Mater.* 26 (31) (2014) 5274–5309.
- [9] W. Fan, M.K. Leung, Recent development of plasmonic resonance-based photocatalysis and photovoltaics for solar utilization, *Molecules* 21 (2) (2016) 180.
- [10] Y. Sun, X. Yang, H. Zhao, R. Wang, Non-symmetric hybrids of noble metal-semiconductor: interplay of nanoparticles and nanostructures in formation dynamics and plasmonic applications, *Prog. Mater Sci. Mater. Int.* 27 (2) (2017) 157–168.
- [11] H. Ahn, H. Song, J. Choi, K. Kim, A localized surface plasmon resonance sensor using double-metal-complex nanostructures and a review of recent approaches, *Sensors* 18 (1) (2018) 98.
- [12] W. Xu, Y. Zhu, X. Chen, J. Wang, L. Tao, S. Xu, T. Liu, H. Song, A novel strategy for improving upconversion luminescence of NaYF4:Yb, Er nanocrystals by coupling with hybrids of silver plasmon nanostructures and poly(methyl methacrylate) photonic crystals, *Nano Res.* 6 (11) (2013) 795–807.
- [13] R. Chikkaraddy, B. De Nijs, F. Ben, S.J. Barrow, O.A. Scherman, E. Rosta, A. Demetriadou, P. Fox, O. Hess, J.J. Baumberg, Single-molecule strong coupling at room temperature in plasmonic nanocavities, *Nature* 535 (7610) (2016) 127–130.
- [14] S.F. Becker, M. Esmann, K. Yoo, P. Gross, R. Vogelgesang, N. Park, C. Lienau, Gap-plasmon-enhanced nanofocusing near-field microscopy, *ACS Photon.* 3 (2) (2016) 223–232.
- [15] H. Xu, E.J. Bjerneld, M. Käll, L. Börjesson, Spectroscopy of single hemoglobin molecules by surface enhanced Raman scattering, *Phys. Rev. Lett.* 83 (21) (1999) 4357.
- [16] H. Xu, J. Aizpurua, M. Käll, P. Apell, Electromagnetic contributions to single-molecule sensitivity in surface-enhanced Raman scattering, *Phys. Rev. E* 62 (3) (2000) 4318.
- [17] E. Hao, G.C. Schatz, Electromagnetic fields around silver nanoparticles and dimers, *J. Chem. Phys.* 120 (1) (2004) 357–366.
- [18] E. Petryayeva, U.J. Krull, Localized surface plasmon resonance: Nanostructures, bioassays and biosensing – a review, *Anal. Chim. Acta* 706 (1) (2011) 8–24.
- [19] Y. Tang, M. Ouyang, Tailoring properties and functionalities of metal nanoparticles through crystallinity engineering, *Nat. Mater.* 6 (10) (2007) 754.
- [20] P.H. Camargo, L. Au, M. Rycenga, W. Li, Y. Xia, Measuring the SERS enhancement factors of dimers with different structures constructed from silver nanocubes, *Chem. Phys. Lett.* 484 (4–6) (2010) 304–308.
- [21] Y. Luo, J. Zhao, Plasmon-exciton interaction in colloidally fabricated metal nanoparticle-quantum emitter nanostructures, *Nano Res.* 12 (9) (2019) 2164–2171.
- [22] Y. Feng, J. He, H. Wang, Y.Y. Tay, H. Sun, L. Zhu, H. Chen, An unconventional role of ligand in continuously tuning of metal-metal interfacial strain, *J. Am. Chem. Soc.* (2012).
- [23] P.R. Mark, Forces and interactions between nanoparticles for controlled structures, *Graduate School-New Brunswick Rutgers, The State University of New Jersey*, 2013 (Ph.D. Thesis).
- [24] W. Li, P.H. Camargo, X. Lu, Y. Xia, Dimers of silver nanospheres: facile synthesis and their use as hot spots for surface-enhanced Raman scattering, *Nano Lett.* 9 (1) (2008) 485–490.
- [25] J.A. Fan, C. Wu, K. Bao, J. Bao, R. Bardhan, N.J. Halas, V.N. Manoharan, P. Nordlander, G. Shvets, F. Capasso, Self-assembled plasmonic nanoparticle clusters, *Science* 328 (2010) 1135–1138.
- [26] E. Cohen-Hoshen, G.W. Bryant, I. Pinkas, J. Sperling, I. Bar-Joseph, Exciton-plasmon interactions in quantum dot-gold nanoparticle structures, *Nano Lett.* 12 (8) (2012) 4260–4264.
- [27] A. Manjavacas, F.J. García de Abajo, P. Nordlander, Quantum plexcitonics: strongly interacting plasmons and excitons, *Nano Lett.* 11 (6) (2011) 2318–2323.
- [28] S. Yampolsky, D.A. Fishman, S. Dey, E. Hulkko, M. Banik, E.O. Potma, V. A. Apkarian, Seeing a single molecule vibrate through time-resolved coherent anti-stokes raman scattering, *Nat. Photon.* 8 (8) (2014) 650–656.
- [29] J. Lermé, Plasmon hybridization model for a nanoparticle above a dielectric interface: dielectric effects, comparison with the dimer system, range of applicability, and limits, *J. Phys. Chem. C* 119 (36) (2015) 21087–21104.
- [30] Y. Huang, L. Ma, M. Hou, J. Li, Z. Xie, Z. Zhang, Hybridized plasmon modes and near-field enhancement of metallic nanoparticle-dimer on a mirror, *Sci. Rep.* 6 (1) (2016) 1–9.
- [31] T.L. Cocker, D. Peller, P. Yu, J. Repp, R. Huber, Tracking the ultrafast motion of a single molecule by femtosecond orbital imaging, *Nature* 539 (7628) (2016) 263–267.
- [32] R. Jin, Y. Cao, C.A. Mirkin, K. Kelly, G.C. Schatz, J. Zheng, Photoinduced conversion of silver nanospheres to nanoprisms, *Science* 294 (5548) (2001) 1901–1903.
- [33] J. Guo, W. Yang, C. Wang, Systematic study of the photoluminescence dependence of thiol-capped CdTe nanocrystals on the reaction conditions, *J. Phys. Chem. B* 109 (37) (2005) 17467–17473.
- [34] A. Mandal, N. Tamai, Influence of acid on luminescence properties of thioglycolic acid-capped CdTe quantum dots, *J. Phys. Chem. C* 112 (22) (2008) 8244–8250.

- [35] S. Gurung, A. Singh, R. Chari, J. Jayabal, The optical response of self-organized Ag-CdTe metal-semiconductor hybrid nanostructures: change in interaction vs number density variation, *J. Appl. Phys.* 124 (20) (2018) 204305.
- [36] C. Strelow, T.S. Theuerholz, C. Schmidtke, M. Richter, J.-P. Merkl, H. Kloust, Z. Ye, H. Weller, T.F. Heinz, A. Knorr, et al., Metal-Semiconductor nanoparticle hybrids formed by self-organization: a platform to address exciton-plasmon coupling, *Nano Lett.* 16 (8) (2016) 4811–4818.
- [37] Y. Wang, M. Li, H. Jia, W. Song, X. Han, J. Zhang, B. Yang, W. Xu, B. Zhao, Optical properties of Ag/CdTe nanocomposite self-organized by electrostatic interaction, *Spectrochim. Acta A* 64 (1) (2006) 101–105.
- [38] N. Mondal, A. Samanta, Ultrafast charge transfer and trapping dynamics in a colloidal mixture of similarly charged CdTe quantum dots and silver nanoparticles, *J. Phys. Chem. C* 120 (1) (2015) 650–658.
- [39] D. Paramelle, A. Sadovoy, S. Gorelik, P. Free, J. Hobley, D.G. Fernig, A rapid method to estimate the concentration of citrate capped silver nanoparticles from UV-visible light spectra, *Analyst* 139 (19) (2014) 4855–4861.
- [40] S.F. Wuister, F. Van Driel, A. Meijerink, Luminescence of CdTe nanocrystals, *J. Lumin.* 102 (2003) 327–332.
- [41] W.W. Yu, L. Qu, W. Guo, X. Peng, Experimental determination of the extinction coefficient of CdTe, CdSe, and CdS nanocrystals, *Chem. Mater.* 15 (14) (2003) 2854–2860.
- [42] W. Chen, A.G. Joly, D.E. McCready, Upconversion luminescence from CdSe nanoparticles, *J. Chem. Phys.* 122 (22) (2005) 224708.
- [43] M.I. Sriram, S.B.M. Kanth, K. Kalishwaralal, S. Gurunathan, Antitumor activity of silver nanoparticles in Dalton's lymphoma ascites tumor model, *Int. J. Nanomed.* 5 (2010) 753–762.
- [44] J. Chang, Y. Ogomi, C. Ding, Y.H. Zhang, T. Toyoda, S. Hayase, K. Katayama, Q. Shen, Ligand-dependent exciton dynamics and photovoltaic properties of PbS quantum dot heterojunction solar cells, *Phys. Chem. Chem. Phys.* 19 (9) (2017) 6358–6367.
- [45] S.A. Gallagher, S. Comby, M. Wojdyla, T. Gunnlaugsson, J.M. Kelly, Y.K. Gun'ko, I. P. Clark, G.M. Greetham, M. Towrie, S.J. Quinn, Efficient quenching of TGA-capped CdTe quantum dot emission by a surface-coordinated europium (III) cyclen complex, *Inorg. Chem.* 52 (8) (2013) 4133–4135.
- [46] J. Jayabal, A. Singh, R. Chari, H. Srivastava, P. Mukhopadhyay, A. Srivastava, S. Oak, Aggregated nanoplatelets: optical properties and optically induced deaggregation, *J. Phys. Condens. Matter* 20 (44) (2008) 445222.
- [47] H.H. Salih, A.M. El Badawy, T.M. Tolaymat, C.L. Patterson, Removal of stabilized silver nanoparticles from surface water by conventional treatment processes, *Adv. Nanomat.* 8 (2019) 21–35.
- [48] M. Mishchenko, Light scattering by randomly oriented axially symmetric particles, *J. Opt. Soc. Am. A* 8 (6) (1991) 871–882.
- [49] D.W. Mackowski, M.I. Mishchenko, Calculation of the T matrix and the scattering matrix for ensembles of spheres, *J. Opt. Soc. Am. A* 13 (11) (1996) 2266–2278.
- [50] P.B. Johnson, R.W. Christy, Optical constants of the noble metals, *Phys. Rev. B* 6 (12) (1972) 4370.
- [51] M. Alves-Santos, R.D. Felice, G. Goldoni, Dielectric functions of semiconductor nanoparticles from the optical absorption spectrum: the case of CdSe and CdS, *J. Phys. Chem. C* 114 (9) (2010) 3776–3780.
- [52] K.L. Kelly, E. Coronado, L.L. Zhao, G.C. Schatz, The optical properties of metal nanoparticles: the influence of size, shape, and dielectric environment, *J. Phys. Chem. B* 107 (2003) 668–677.
- [53] L. Genzel, T. Martin, U. Kreibig, Dielectric function and plasma resonances of small metal particles, *Z. Phys. B: Condens. Matter* 21 (4) (1975) 339–346.
- [54] J.J. Mock, D.R. Smith, S. Schultz, Local refractive index dependence of plasmon resonance spectra from individual nanoparticles, *Nano Lett.* 3 (4) (2003) 485–491.
- [55] K.G. Stamplecoskie, J.C. Sciaiano, Kinetics of the formation of silver dimers: early stages in the formation of silver nanoparticles, *J. Am. Chem. Soc.* 133 (11) (2011) 3913–3920.
- [56] M. Grouchko, A. Kamysny, C.F. Mihailescu, D.F. Anghel, S. Magdassi, Conductive inks with a “built-in” mechanism that enables sintering at room temperature, *ACS Nano* 5 (4) (2011) 3354–3359.
- [57] M. Grouchko, P. Roitman, X. Zhu, I. Popov, A. Kamysny, H. Su, S. Magdassi, Merging of metal nanoparticles driven by selective wettability of silver nanostructures, *Nat. Commun.* 5 (2014) 2994.
- [58] N.J. Halas, S. Lal, W.-S. Chang, S. Link, P. Nordlander, Plasmons in strongly coupled metallic nanostructures, *Chem. Rev.* 111 (6) (2011) 3913–3961.
- [59] P. Mariano, M. Giovanni, T. Robert, C. Forestiere, Full-wave electromagnetic modes and hybridization in nanoparticle dimers, *Sci. Rep.* 9 (2019) 14524.
- [60] C. Guillou, P. Langot, N. Del Fatti, F. Vallee, Ultrafast surface plasmon resonance landau damping and electron kinetics in metal nanoparticles, *Ultrafast Phenomena in Semiconductors and Nanostructure Materials VIII* 5352 (2004) 65–76.
- [61] A. Singh, S. Gurung, R. Chari, J. Jayabal, Counting the electrons hopping in ultrafast time scales in an Ag-CdTe hybrid nanostructure, *J. Phys. Chem. C* 123 (2019) 28584–28592.
- [62] N. Del Fatti, C. Voisin, M. Achermann, S. Tzortzakis, D. Christofilos, F. Vallée, Nonequilibrium electron dynamics in noble metals, *Phys. Rev. B* 61 (24) (2000) 16956.
- [63] J.-Y. Bigot, V. Halté, J.-C. Merle, A. Daunois, Electron dynamics in metallic nanoparticles, *Chem. Phys.* 251 (1–3) (2000) 181–203.
- [64] J. Jayabal, Origin and time dependence of higher-order nonlinearities in metal nanocomposites, *J. Opt. Soc. Am. B* 28 (10) (2011) 2448–2455.
- [65] M. Perner, S. Gresillon, J. März, G. Von Plessen, J. Feldmann, J. Porstendorfer, K.-J. Berg, G. Berg, Observation of hot-electron pressure in the vibration dynamics of metal nanoparticles, *Phys. Rev. Lett.* 85 (4) (2000) 792.
- [66] R. Sato, M. Ohnuma, K. Oyoshi, Y. Takeda, Experimental investigation of nonlinear optical properties of ag nanoparticles: effects of size quantization, *Phys. Rev. B* 90 (12) (2014) 125417.
- [67] P.K. Jain, W. Qian, M.A. El-Sayed, Ultrafast electron relaxation dynamics in coupled metal nanoparticles in aggregates, *J. Phys. Chem. B* 110 (1) (2006) 136–142.
- [68] M.J. Feldstein, C.D. Keating, Y.-H. Liu, M.J. Natan, N.F. Scherer, Electronic relaxation dynamics in coupled metal nanoparticles, *J. Am. Chem. Soc.* 119 (28) (1997) 6638–6647.
- [69] X.-C. Yang, Z.-W. Dong, H.-X. Liu, J.-X. Xu, S.-X. Qian, Effects of thermal treatment on the third-order optical nonlinearity and ultrafast dynamics of Ag nanoparticles embedded in silicate glasses, *Chem. Phys. Lett.* 475 (4–6) (2009) 256–259.
- [70] K. Wu, J. Chen, J.R. McBride, T. Lian, Efficient hot-electron transfer by a plasmon-induced interfacial charge-transfer transition, *Science* 349 (6248) (2015) 632–635.
- [71] A. Furube, S. Hashimoto, Insight into plasmonic hot-electron transfer and plasmon molecular drive: new dimensions in energy conversion and nanofabrication, *NPG Asia Mater.* 9 (12) (2017) e454.
- [72] B. Gao, Y. Lin, S. Wei, J. Zeng, Y. Liao, L. Chen, D. Goldfeld, X. Wang, Y. Luo, Z. Dong, J. Hou, Charge transfer and retention in directly coupled Au-CdSe nanohybrids, *Nano Res.* 5 (2) (2012) 88–98.
- [73] Y. Tang, Z. Jiang, G. Xing, A. Li, P.D. Kanhere, Y. Zhang, T.C. Sum, S. Li, X. Chen, Z. Dong, et al., Efficient Ag@AgCl cubic cage photocatalysts profit from ultrafast plasmon-induced electron transfer processes, *Adv. Funct. Mater.* 23 (23) (2013) 2932–2940.
- [74] J.K. Vaishnav, T.K. Mukherjee, Long-range resonance coupling-induced surface energy transfer from CdTe quantum dot to plasmonic nanoparticle, *J. Phys. Chem. C* 122 (49) (2018) 28324–28336.
- [75] A. Ragab, A.-S. Gadallah, M. Mohamed, I. Azzouz, Photoluminescence and upconversion on Ag/CdTe quantum dots, *Opt. Laser Technol.* 63 (2014) 8–12.
- [76] Z. Bian, T. Tachikawa, P. Zhang, M. Fujitsuka, T. Majima, Au/TiO<sub>2</sub> superstructure-based plasmonic photocatalysts exhibiting efficient charge separation and unprecedented activity, *J. Am. Chem. Soc.* 136 (1) (2013) 458–465.
- [77] D. Radziuk, H. Moehwald, Prospects for plasmonic hot spots in single molecule SERS towards the chemical imaging of live cells, *Phys. Chem. Chem. Phys.* 17 (33) (2015) 21072–21093.
- [78] E.-M. Roller, L.V. Besteiro, C. Pupp, L.K. Khorashad, A.O. Govorov, T. Liedl, Hotspot-mediated non-dissipative and ultrafast plasmon passage, *Nat. Phys.* 13 (8) (2017) 761.